CHEMISTRY OF MATERIALS
Article

Chem. Mater. **2010,** *22,* 4495–4504 4495
DOI:10.1021/cm101436p

Exploring the Limitations of the Use of Competing Reducers to Control the Morphology and Composition of Pt and PtCo Nanocrystals

Stephanie I. Lim,[†] Miriam Varón,[†] Isaac Ojea-Jiménez,[†] Jordi Arbiol,[‡,§] and Victor Puntes*[,†,§]

[†]*Institut Català de Nanotecnologia, Barcelona, Spain,* [‡]*Institut de Ciència de Materials de Barcelona, CSIC, Barcelona, Spain, and* [§]*Institut Català de Recerca i Estudis Avançats* (*ICREA*)*, Barcelona, Spain*

Received May 21, 2010. Revised Manuscript Received June 18, 2010

We have explored size- and shape-controlled synthesis of platinum nanocrystals (Pt NCs) by systematically comparing the differential reducing performance of two competing reducing agents in a one-pot synthesis: hexadecanediol, a weak reducer, and metallic cobalt or superhydride, stronger reducers of Pt. In addition to its role as a metal reducer, Co also functions as a shape-directing agent and is incorporated into the Pt NCs, forming a PtCo alloy structure. By maintaining a constant HDD concentration and systematically increasing the Co content, the shape of the resulting NCs was found to alter from polypods, when no Co was present, to cuboctahedrons and cubes when trace amounts of Co were added, and back to polypods when Co dominated the reduction process. On the other hand, when the concentration of HDD was systematically increased (with Co kept constant), evolution from polypod morphology to prismatic/spherical/cubic NCs, followed by irregular shapes was observed. Both experimental results indicate the importance of the competitive role between the reducing agents, their concentration limits for achieving a controlled morphology, and the presence of Co as a shape-directing agent to alter the NC shape. This allows the exploration of a wide range of NC morphologies without significant modification of the synthesis recipe.

Introduction

The basic components needed for a nanocrystal (NC) wet-synthesis include a metal precursor, a surfactant agent (also known as a stabilizing or templating agent), and a reducing agent. With the increasing interest in the fabrication of robust colloidal NCs with controllable size, shape, and composition, many syntheses have been extended to the use of two or more metals, creating alloys or hybrid NCs[1−4] in the presence of one or two surfactant agents (e.g., alkyl thiols,[5] carboxylic acid,[6] amines,[7,8] phosphine,[9] or polyol[10,11]), making the reaction mixtures more complex. In some cases, the surfactant is also used as a reducer, as illustrated in the synthesis of Au with sodium citrate,[12] or as a solvent in the case of CdSe with trioctyl phosphine oxide.[1a] On rare occasions, two reducing agents are required, as in the case of hydroquinone, where the initial reduction of a small fraction of Ag ions has to be instigated by another reducer before hydroquinone can reduce the remaining Ag ions for NC growth,[13] or the use of ascorbic acid to reduce Au^{3+} to Au^{+}, followed by subsequent reduction using Au seeds for the synthesis of Au nanorods.[7b] However, in these cases, the reducers were employed in a sequential manner rather than having a competitive role. In general, the kinetics of a NC synthesis can be manipulated by changing the concentration, temperature, reducing power, and additives/surfactants, which produce complex intermediates that accelerate or slow down the precursor reduction, affecting both the nucleation rate and the nuclei stability.

*To whom correspondence should be addressed. E-mail: victor.puntes.icn@uab.es.

(1) (a) Peng, X.; Manna, L.; Yang, W.; Wickham, J.; Scher, E.; Kadavanich, A.; Alivisatos, A. P. *Nature* **2000**, *404*, 59. (b) Luther, J. M.; Zheng, H.; Sadtler, B.; Alivisatos, A. P. *J. Am. Chem. Soc.* **2009**, *131*, 16851. (c) Yin, Y.; Alivisatos, A. P. *Nature* **2005**, *437*, 664.
(2) (a) Skrabalak, S. E.; Xia, Y. *ACS Nano* **2009**, *3*, 10. (b) Lim, B.; Wang, J.; Camargo, P. H. C.; Jiang, M.; Kim, M. J.; Xia, Y. *Nano Lett.* **2008**, *8*, 2535. (c) Cho, E. C.; Camargo, P. H. C.; Xia, Y. *Adv. Mater.* **2010**, *22*, 744.
(3) (a) Cozzoli, P. D.; Pellegrino, T.; Manna, L. *Chem. Soc. Rev.* **2006**, *35*, 1195. (b) Figuerola, A.; Fiore, A.; Corato, R. D.; Falqui, A.; Giannini, C.; Micotti, E.; Lascialfari, A.; Corti, M.; Cingolani, R.; Pellegrino, T.; Cozzoli, P. D.; Manna, L. *J. Am. Chem. Soc.* **2008**, *130*, 1477.
(4) (a) Sun, S. *Adv. Mater.* **2006**, *18*, 393. (b) Yu, H.; Chen, M.; Rice, P. M.; Wang, S. X.; White, R. L.; Sun, S. *Nano Lett.* **2005**, *5*, 379.
(5) Shichibu, Y.; Negishi, Y.; Tsunoyama, H.; Kanehara, M.; Teranishi, T.; Tsukuda, T. *Small* **2007**, *3*, 835.
(6) Dinh, C.-T.; Nguyen, T.-D.; Kleitz, F.; Do, T.-O. *ACS Nano* **2009**, *3*, 3737.
(7) (a) Murphy, C. J.; Gole, A. M.; Hunyadi, S. E.; Orendorff, C. J. *Inorg. Chem.* **2006**, *45*, 7544. (b) Jana, N. R.; Gearheart, L.; Murphy, C. J. *J. Phys. Chem. B* **2001**, *105*, 4065.
(8) Fink, J.; Kiely, C. J.; Bethell, D.; Schiffrin, D. J. *Chem. Mater.* **1998**, *10*, 922.
(9) (a) Puntes, V. F.; Krishnan, K. M.; Alivisatos, A. P. *Science* **2001**, *291*, 2115. (b) Puntes, V. F.; Zanchet, D.; Erdonmez, C. K.; Alivisatos, A. P. *J. Am. Chem. Soc.* **2002**, *124*, 12874.
(10) (a) Cobley, C. M.; Campbell, D. J.; Xia, Y. *Adv. Mater.* **2008**, *20*, 748. (b) Lu, X.; Au, L.; McLellan, J.; Li, Z.; Marquez, M.; Xia, Y. *Nano Lett.* **2007**, *7*, 1764.
(11) Seo, D.; Park, J. C.; Song, H. *J. Am. Chem. Soc.* **2006**, *128*, 14863.
(12) Turkevich, J.; Stevenson, P. C.; Hillier, J. *J. Phys. Chem.* **1953**, *57*, 670.
(13) Gentry, S. T.; Fredericks, S. J.; Krchnavek, R. *Langmuir* **2009**, *25*, 2613.

Published on Web 07/19/2010

Despite numerous reports on the importance of kinetic control in NC growth, mixtures of reducers to accelerate the reduction of a fraction of the precursor at a desired moment during the nucleation−growth process have not been explored.

One of the reasons for perfecting and understanding the nature of colloidal NC synthesis is their efficacy in a wide variety of applications.[14−17] For example, platinum (Pt) NCs have been intensely researched in areas of plasmonic and fuel cell catalysis because of their novel and effective optical and catalytic properties that are of vital importance in the development of new "greener" technologies.[18−21] Ever since El Sayed[22] and Somorjai[23] demonstrated how Pt shaped NCs can affect the selectivity and activity in a catalytic reaction (because of the ability to expose a specific set of facets), a considerable number of reports describing different approaches to the synthesis of shaped Pt NCs have emerged.[24−28] Recently, our group reported the shape-control of Pt NCs in the presence of different Co traces and other metals at one constant concentration ($< 5\%$).[29] As discussed, in addition to the weak reducing agent (Hexadecanediol, HDD), a Co trace can function as both a metal reducer and shape directing agent. The use of metals as reducers was also recently reported by Zou et al. where tungsten (not at a trace concentration) was added as a foreign element to reduce the Pt precursor.[30] The authors reported that without $W(CO)_6$, Pt_3Ni NCs could still be produced, but their morphology appeared to be much less controlled, indicating again the influence of kinetic control on NC morphology.

While the concept of shape-control is not new, the process by which it occurs is still not fully understood. In this work, we explore the synthesis of Pt NCs in the presence of Co^0 with a broad range of reducer compositions and concentrations. Intentional and systematic use of two competing reducers in a one-pot synthesis to kinetically control the NC growth, until now, has remained unexplored. In addition, while atomic traces such as Br^-, Ag^+, and Fe^{2+} have been utilized for shape control,[24−26] the use of NCs as a means of introducing metallic ions into the synthesis has not been reported other than in our recently published work.[29] Here, beyond the previous results, we show that Pt and PtCo alloy NCs with different morphologies can be obtained by systematically varying the concentration of two competing reducing agents, hexadecanediol and metallic Co, while maintaining an otherwise fixed set of reaction conditions. Our results demonstrate, in particular, the importance of the competitive relationship between the two different reducers, how the NC growth toward a particular shape can be influenced at a very early stage, as well as the importance of exploring the kinetic and concentration limits to achieve a controlled morphology. Unlike other size-controlled NC syntheses, where spherical NCs of 1−100 nm are obtained by varying the precursor/reducer ratio,[31] chain lengths of capping agents[32] or changing the reaction temperatures,[33] our results reveal a change in both the *shape* and the *size* of the NCs as we vary the Co and HDD concentrations. Experiments in the absence of metallic Co or using a stronger reducing agent such as lithium triethylborohydride confirmed the proposed mechanism.

Experimental Procedures

Chemicals. Platinum(II) acetylacetonate ($Pt(acac)_2$, 98%) was purchased from Strem Chemicals and used as received. Oleylamine (OAM, 70%), 1,2-dichlorobenzene anhydrous (DCB, 99%), 1,2-hexadecanediol (HDD, 90%), superhydride lithium triethylborohydride (in 1 M THF) and cobalt carbonyl moistened with 5−10% hexane ($Co_2(CO)_8$, 90−95%) were purchased from Sigma-Aldrich and used as received. All chemicals

(14) (a) Wu, Y.; Wadia, C.; Ma, W.; Sadtler, B.; Alivisatos, A. P. *Nano Lett*. **2008**, *8*, 2551. (b) Alivisatos, A. P. *Nat. Biotechnol*. **2004**, *22*, 47.
(15) (a) Wang, H.; Brandl, D. W.; Nordlander, P.; Halas, N. J. *Acc. Chem. Res*. **2007**, *40*, 53. (b) Lal, S.; Grady, N. K.; Kundu, J.; Levin, C. S.; Lassiter, J. B.; Halas, N. J. *Chem. Soc. Rev*. **2008**, *37*, 898.
(16) Thomas, K. G.; Kamat, P. V. *Acc. Chem. Res*. **2003**, *36*, 888.
(17) (a) Petrova, H.; Lin, C.-H.; Hu, M.; Chen, J.; Siekkinen, A. R.; Xia, Y.; Sader, J. E.; Hartland, G. V. *Nano Lett*. **2007**, *7*, 1059. (b) Li, Z.-Y.; Xia, Y. *Nano Lett*. **2010**, *10*, 243. (c) Jeong, U.; Teng, X.; Wang, Y.; Yang, H.; Xia, Y. *Adv. Mater*. **2007**, *19*, 33.
(18) (a) Xiong, Y.; Wiley, B. J.; Xia, Y. *Angew. Chem., Int. Ed*. **2007**, *46*, 7157. (b) Chen, J.; Lim, B.; Lee, E. P.; Xia, Y. *Nano Today* **2009**, *4*, 81. (c) Xia, Y.; Xiong, Y.; Lim, B.; Skrabalak, S. E. *Angew. Chem., Int. Ed*. **2009**, *48*, 60.
(19) Zhong, C. J.; Luo, J.; Njoki, P. N.; Mott, D.; Wanjala, B.; Loukrakpam, R.; Lim, S. I.; Wang, L.; Fang, B.; Xu, Z. *Energy Environ. Sci*. **2008**, *1*, 454.
(20) Tian, N.; Zhou, Z.-Y.; Sun, S.-G. *J. Phys. Chem. C* **2008**, *112*, 19801.
(21) (a) Subhramannia, M.; Ramaiyan, K.; Pillai, V. K. *Langmuir* **2008**, *24*, 3576. (b) Subhramannia, M.; Pillai, V. K. *J. Mater. Chem*. **2008**, *18*, 5858.
(22) (a) Ahmadi, T. S.; Wang, Z. L.; Green, T. C.; Henglein, A.; El-Sayed, M. A. *Science* **1996**, *272*, 1924. (b) Narayanan, R.; El-Sayed, M. A. *J. Am. Chem. Soc*. **2004**, *126*, 7194.
(23) Bratlie, K. M.; Lee, H.; Komvopoulos, K.; Yang, P.; Somorjai, G. A. *Nano Lett*. **2007**, *7*, 3097.
(24) (a) Chen, J.; Herricks, T.; Xia, Y. *Angew. Chem., Int. Ed*. **2005**, *44*, 2589. (b) Chen, J.; Herricks, T.; Geissler, M.; Xia, Y. *J. Am. Chem. Soc*. **2004**, *126*, 10854. (c) Lim, B.; Lu, X.; Jiang, M.; Camargo, P. H. C.; Cho, E. C.; Lee, E. P.; Xia, Y. *Nano Lett*. **2008**, *8*, 4043. (d) Herricks, T.; Chen, J.; Xia, Y. *Nano Lett*. **2004**, *4*, 2367.
(25) (a) Tsung, C.; Kuhn, J. N.; Huang, W.; Aliaga, C.; Hung, L.; Somorjai, G. A.; Yang, P. *J. Am. Chem. Soc*. **2009**, *131*, 5816. (b) Song, H.; Kim, F.; Connor, S.; Somorjai, G. A.; Yang, P. *J. Phys. Chem. B* **2005**, *109*, 188.
(26) (a) Wang, C.; Daimon, H.; Lee, Y.; Kim, J.; Sun, S. *J. Am. Chem. Soc*. **2007**, *129*, 6974. (b) Wang, C.; Daimon, H.; Onodera, T.; Koda, T.; Sun, S. *Angew. Chem*. **2008**, *120*, 3644.
(27) (a) Ren, J.; Tilley, R. D. *J. Am. Chem. Soc*. **2007**, *129*, 3287. (b) Ren, J.; Tilley, R. D. *Small* **2007**, *3*, 1508. (c) Cheong, S.; Watt, J.; Ingham, B.; Toney, M. F.; Tilley, R. D. *J. Am. Chem. Soc*. **2009**, *131*, 14590.
(28) (a) Mahmoud, M. A.; Tabor, C. E.; El-Sayed, M. A.; Ding, Y.; Wang, Z. L. *J. Am. Chem. Soc*. **2008**, *130*, 4590. (b) Tian, N.; Zhou, Z.-Y.; Sun, S.-G.; Ding, Y.; Wang, Z. L. *Science* **2007**, *316*, 732. (c) Zhang, H.-T.; Ding, J.; Chow, G.-M. *Langmuir* **2008**, *24*, 375. (d) Tzitzios, V.; Niarchos, D.; Gjoka, M.; Boukos, N.; Petridis, D. *J. Am. Chem. Soc*. **2005**, *127*, 13756. (e) Demortiere, A.; Launois, P.; Goubet, N.; Albouy, P.-A.; Petit, C. *J. Phys. Chem. B* **2008**, *112*, 14583. (f) Teng, X.; Yang, H. *Nano Lett*. **2005**, *5*, 885. (g) Shevchenko, E. V.; Talapin, D. V.; Schnablegger, H.; Kornowski, A.; Festin, O.; Svedlindh, P.; Haase, M.; Weller, H. *J. Am. Chem. Soc*. **2003**, *125*, 9090.
(29) Lim, S. I.; Ojea-Jimenez, I.; Varon, M.; Casals, E.; Arbiol, J.; Puntes, V. *Nano Lett*. **2010**, *10*, 964.
(30) Zhang, J.; Yang, H.; Fang, J.; Zou, S. *Nano Lett*. **2010**, *10*, 638.
(31) Chen, G.; Takezawa, M.; Kawazoe, N.; Tateishi, T. *Open Biotechnol. J*. **2008**, *2*, 152.
(32) Schadt, M. J.; Cheung, W.; Luo, J.; Zhong, C. J. *Chem. Mater*. **2006**, *18*, 5147.
(33) (a) Peng, S.; Lee, Y.; Wang, C.; Yin, H.; Dai, S.; Sun, S. *Nano Res*. **2008**, *1*, 229. (b) Zheng, N.; Fan, J.; Stucky, G. D. *J. Am. Chem. Soc*. **2006**, *128*, 6550.

were stored and prepared for synthesis in a UNIlab MBraun glovebox unless otherwise stated.

Instrumentation. Transmission electron microscopy (TEM) analysis was performed on a JEOL 1010 with an accelerating voltage of 80 kV. High resolution TEM (HRTEM) analysis was performed on a JEOL 2010F field emission gun microscope. The 3D supercell atomic models were designed by using the Rhodius software package available online at the University of Cadiz.[34] In general, the supercell atomic models created are composed of 6000 to 25000 Pt atoms, and correspond to the same diameters as the experimental crystals found. Energy-dispersive X-ray (EDX) analysis was performed on a JEOL 2100 with an accelerating voltage of 200 kV equipped with an EDX detector. The NCs were drop-cast onto a carbon coated grid and allowed to air-dry under ambient conditions. X-ray diffraction (XRD) data were collected on a PANalytical ẊPert diffractometer using a Cu Kα radiation source (λ = 1.541 Å). In a typical experiment, the 2θ diffraction (Bragg) angles were measured by scanning the goniometer from 25° to 100° at a speed of 0.021° s^{-1}. The samples were prepared by precipitating the NCs in the presence of methanol followed by brief centrifugation to ensure that all the NCs precipitated. The supernatant was discarded, and the samples were dried under nitrogen before smearing onto (510) silicon wafers (3° off axis) for XRD analysis. Estimates of NC size were obtained using the Scherrer equation ($d = (K\lambda)/\beta\cos\theta$) where d is the mean crystallite dimension, K is the shape factor (0.9), λ is the X-ray wavelength, β is the line broadening at full width at half-maximum (fwhm, radians), and θ is the Bragg angle. The peak positions were determined using the ẊPert HighScore program and compared before and after baseline correction. Calculations using Vegard's law support the observed shifts in the 2θ Bragg peaks when compared to those for pure Pt and Co NCs. Induced coupled plasma-mass spectroscopy (ICP-MS) was performed using an ICP-MS Agilent instrument (Model: 7500cx) with a detection limit of 0.02386 ppb. Aliquots of the purified NC samples were dissolved in concentrated aqua regia, which was heated to ensure complete dissolution of all metals, and diluted to an optimal concentration for ICP-MS analysis. Ga was used as the internal standard, and the integration time/point and time/mass were 0.1 and 0.3 s, respectively, with a 3× repetition.

Synthesis. Unless otherwise stated, all syntheses were performed under an argon atmosphere using the standard Schlenk-line setup to avoid interactions between the NCs and O_2, H^+, or ^-OH species, and the $Pt(acac)_2$ concentration was constant in all syntheses. To remove the excess capping, reducing agent or ions, the PtCo NCs were purified by precipitation in methanol followed by brief centrifugation and redispersion in DCB prior to being subjected to further analysis (XRD, ICP-MS, EDX).

Increasing Cobalt Content. In the synthesis where the concentration of HDD remained constant while the Co concentration was systematically increased, a solution containing 95 mg of HDD (0.37 mmol), 45 μL of OAM, and 10 mL of DCB was added to a 3-neck round-bottom flask equipped with a condenser and stirred under an argon atmosphere. The solution temperature was increased to 180 °C using a glycerol oil bath over a time period of ~30−60 min. Once the boiling temperature of DCB was reached, a 3 mL solution of DCB containing 45 mg of $Pt(acac)_2$ (0.11 mmol) was added dropwise at a rate of 0.5 mL/min. A 100 μL portion of Co trace prepared from $Co_2(CO)_8$ (ranging from 0 to 54 μmol) was then added immediately to the solution. The solution was refluxed at 180 °C for 20 min and gradually cooled down to room temperature before being transferred to an argon filled vial.

Increasing Hydride Content. In a set of control syntheses, the Co was replaced with a stronger reducing agent, lithium triethylborohydride. In this case, the HDD amount remained constant at 0.37 mmol while the hydride concentration was varied from 0.2 to 40 μmol (taken at 100 μL each time). The remaining synthesis was conducted following the method described above.

Increasing HDD Content. In the synthesis where the concentration of HDD was varied while maintaining a constant Co concentration, different amounts of HDD ranging from 0 to 1.5 mmol, and a constant concentration of Co trace prepared from $Co_2(CO)_8$ (100 μL containing 2.2 μmol of Co) were added to the synthesis following the method described above.

Results and Discussion

Under the reported condition, hexadecanediol (HDD) is added along with oleylamine (OAM) and dichlorobenzene (DCB) at room temperature before increasing the temperature of the solution to 180 °C when the Pt precursor is added. The addition of Pt ions (dropwise at a rate of 0.5 mL/min) to the refluxing solution enables HDD to drive the reducing process. The color of the solution remains yellowish to yellow-green for 5−10 min, implying a mixture of the Pt ions with some partially reduced Pt nuclei. If the reaction is left undisturbed during the remaining reaction time (20 min), Pt polypods are obtained, together with a color evolution to black. However, if a small amount of $Co_2(CO)_8$ (< 5%) is added right after the addition of the Pt precursor, a color evolution to brown occurs much faster, and cubic or octahedral NCs are obtained. The role of metallic Co is complex and can be introduced into the synthesis as $Co_2(CO)_8$ or Co NCs. In this case, the $Co_2(CO)_8$ is assumed to be temporally decomposed to form Co NCs before being oxidized by the reduction of the Pt ions, and it is later reduced back to metallic Co and incorporated in the Pt, forming PtCo alloy nanostructures.[29] Throughout the study, we use the term "trace" in some cases to represent the small amount of Co added to the synthesis, as this has also been employed in the literature.[24−26]

Using the experimental procedure described above, the reduction of Pt ions was examined in the presence of two competing reducing agents (Co and HDD) with different reducing strengths. While the reduction of Pt^{2+} (Pt^{2+}/Pt, $E°_{red}$ = +1.20 V[35]) has been achieved using HDD under the reported reaction conditions,[29] the exact reduction potential value of HDD is not yet determined. However, it is possible to delimit a reduction potential range by comparing with other reported studies performed under similar conditions, in which HDD was able to reduce Cu^{2+} (Cu^{2+}/Cu, $E°_{red}$ = +0.34 V[36a]) but partially Fe^{2+} (Fe^{2+}/Fe, $E°_{red}$ = −0.44 V[36b]). Besides, the redox potential of Co^{2+} is −0.28 V,[35]

(34) (a) Bernal, S.; Botana, F. J.; Calvino, J. J.; Lopez-Cartes, C.; Perez-Omil, J. A.; Rodriguez-Izquierdo, J. M. *Ultramicroscopy* **1998**, *72*, 135. (b) Pérez-Omil, J. A. Doctoral Thesis, University of Cádiz, Spain, 1994.

(35) (a) Cotton, F.; Wilkinson, G. *Inorg. Chem.*, 4th ed.; Wiley-Interscience: New York, 1980. (b) Hayward, M. A.; Green, M. A.; Rosseinsky, M. J.; Sloan, J. *J. Am. Chem. Soc.* **1999**, *121*, 8843.

(36) (a) Mott, D.; Galkowski, J.; Wang, L.; Luo, J.; Zhong, C. J. *Langmuir* **2007**, *23*, 5740. (b) Sun, S.; Zeng, H. *J. Am. Chem. Soc.* **2002**, *124*, 8204.

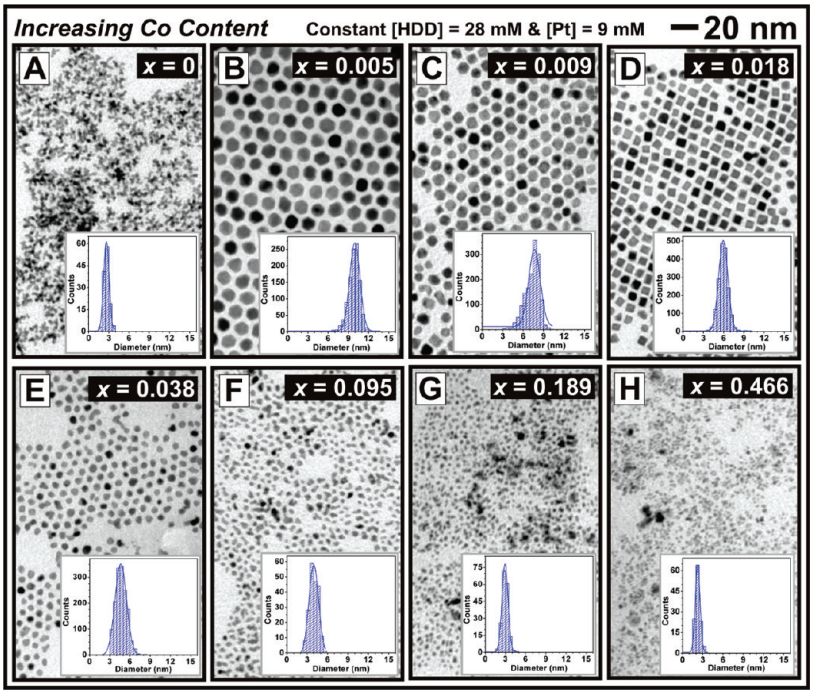

Figure 1. TEM images and the corresponding statistical size analysis of the PtCo NCs synthesized with increasing Co concentrations while maintaining constant HDD and Pt precursor concentrations. The [Co]/[Pt] ratio is represented by x.

Scheme 1. Schematic Diagram Illustrating the Growth Mechanism of Pt (and PtCo) NCs in the Presence of a Sole Reducer (R_1 or R_2) or a Mixture of Reducers (R_1+R_2), Where R_1 Represents HDD and R_2 Represents Co

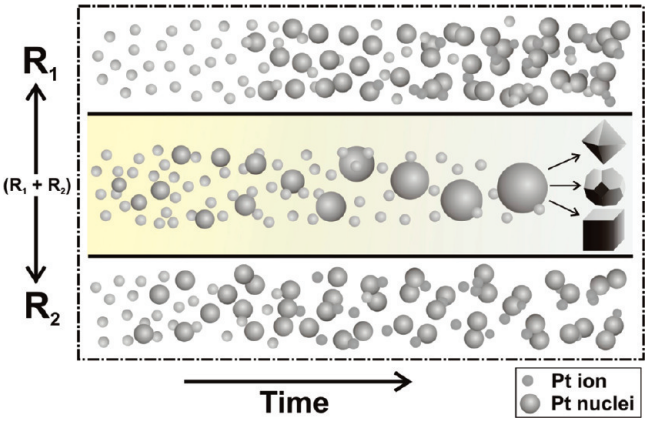

and it can provide a faster and more effective reduction of the Pt ions under the reaction conditions. As shown in Scheme 1 and later confirmed by experimental data, when HDD is present as the sole reducer, there is no competition in the reducing rate, and polypod-type morphology is observed. However, in the presence of both HDD and Co, a competition between the two reducers leads to large, shaped NCs. Depending on the proportion of HDD and Co added in a synthesis, there may be a balanced competition between the two reducers, or one reducer may dominate the other. Eventually, the continued increase in Co concentration leads to an even faster reducing rate and the appearance of flake-like NCs, which are similar to the polypod structures obtained using solely HDD. Experiments substituting superhydride for $Co_2(CO)_8$ show the same behavior, but without the effect of shape-control induced by the Co.

In the following sessions, we carried out systematic experiments where the concentration of only one reducer (whether it be HDD or Co) was varied to examine the resulting effects on both the size and the shape of the NCs. The HDD amounts used ranged from 0 to 1.5 mmol, but because of the strong reduction potential of Co, lower Co amounts of 0−54 μmol were sufficient. Hereon, the reducer concentrations are presented with respect to the Pt precursor concentration, for example, [HDD or Co]/[Pt].

Increasing Co Content. Figure 1 represents TEM images and the corresponding size distribution analyses when different amounts of metallic Co were added to the syntheses while maintaining constant HDD and Pt precursor concentrations. The increase in Co concentration is represented by the value of x, which is determined from the ratio of [Co]/[Pt]. As illustrated in Figure 1A, polypod (or multipod) structures were observed when HDD was presented as the sole reducer in the synthesis ([Co] = 0). The polypods exhibited a multiarmed morphology, where each arm comprised small cemented Pt NCs.[29] This morphology diminished when Co was added to the synthesis, as illustrated by the morphological change from polypod to cuboctahedron PtCo NCs in Figure 1B. The size distribution analysis shows a sharp increase in the NC size from 2.7 nm (Figure 1A) to 9.8 nm (Figure 1B). This dramatic change illustrates the effect of having two differential reducers in a one-pot synthesis, even with a small amount of Co.

The increase in Co content from x = 0.005 to 0.038 further altered the NC shape as Co began to play a more prominent role as a reducer and shape-directing agent. This is represented by the shape evolution of PtCo NCs into spherical and cubic morphologies shown in Figures 1B to 1E, with NC sizes ranging from 7.3 nm (Figure 1C) to 4.7 nm (Figure 1E). The

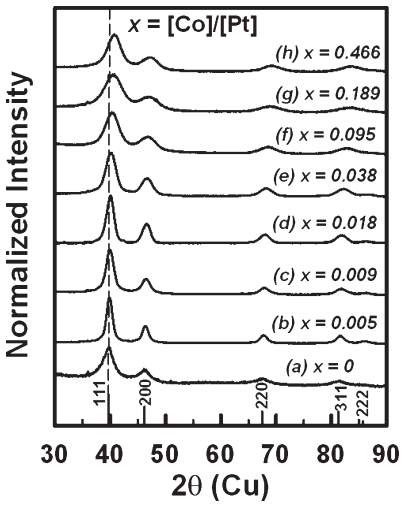

Figure 2. XRD patterns for the PtCo NCs synthesized in the presence of increasing Co content (x = [Co]/[Pt]) with constant HDD and Pt precursor concentrations.

increasing Co content from $x = 0.095$ to 0.466 gave rise to an even faster Pt ion reduction, and resulted in the disappearance of the monodispersed shapes and the appearance of irregular shaped and flake-like NCs (Figure 1, panels G and H), which appear similar to those in Figure 1A obtained using only HDD as the reducer. The polycrystalline polypods and flake-like NCs have average crystal sizes ranging from 3.9 (Figure 1F) to 2.3 nm (Figure 1H). To understand the growth mechanism, it is useful to monitor the size distribution of the NCs since it provides a fingerprint of their growing process. The full width at half-maximum (fwhm) of the fitted Gaussian functions in the statistical size distribution analysis data shows an initial increase in the size dispersion, followed by a momentary decrease that corresponds to the monodispersed cubic PtCo NCs in Figure 1D (see Supporting Information, Figure S1). Monodispersity is related to the homogeneous growth as described in the *growth-by-diffusion* work of Reiss et al.,[37] and later referred to as *size-focusing* by Alivisatos et al.[38] A region of the highly ordered cubes was analyzed by fast-Fourier transform (FFT), where the size of the cubes and interparticle distance between neighboring NCs were estimated to be 6.1 and 2.8 nm, respectively (Supporting Information, Figure S2).

The PtCo alloys were further analyzed using XRD, showing the evolution of their crystalline structure as the Co content increased. The 2θ Bragg peaks in Figure 2 correspond to the known (111), (200), (220), (311), and (222) reflections of the Pt face-centered cubic structure (JCPDS no. 04-0802). As illustrated by the dotted line, there is a slight shift in the measured 2θ Bragg peaks as x varies from 0 (a) to 0.466 (h), which can be attributed to a compression of the Pt crystal lattice because of the incorporation of increasing amounts of Co into the NC structure forming a solid solution. Using Vegard's law, the Co content (with respect to Pt) was calculated by comparing the lattice parameters (a) obtained from the measured 2θ Bragg peaks with those of pure Pt NCs (a = 3.917 Å) and Co NCs (a = 3.533 Å).[39] These experimentally determined values were also compared to the theoretical % Co added to a synthesis, along with elemental composition analysis from ICP-MS (Table 1). As x increases from 0 to 0.466, the theoretical Co content added to the synthesis increases from 0 to 31.8%, which is in good agreement with the trend obtained from XRD and ICP-MS. However, a higher fraction of Co in the NCs was consistently observed in both XRD and ICP-MS, indicating a difference in the Pt to Co proportion in the NCs and in solution, since not all of the Pt^{2+} was reduced to Pt^0 (the unreacted Pt^{2+} remained in the supernatant in ionic form) while a majority of the Co was incorporated in the Pt NCs. This also implies that under these reaction conditions, the conversion rate of Pt ions to Pt^0 is lower than that for Co (typically ~40% Pt yield from ICP-MS). The slightly lower % Co obtained from XRD when $x = 0.466$ (25.7%) may be due to the low signal-to-noise ratio and peak broadening effects, owing to the small size of the NC domains. The increase in % Co was also confirmed by EDX analysis (Supporting Information, Figure S3). The ensemble of data suggests that during synthesis, the metallic Co reduces the Pt^{2+} ions and in the process becomes oxidized. The incorporation of Co into the Pt NCs as a metal further suggests that the oxidized Co is later reduced back to Co^0, probably with the assistance of the Pt NCs as a catalyst.

Table 1. Tabulated Comparison of the Atomic % of Co (with Respect to Pt) Obtained from the Theoretical Synthesis, Calculated from Vegard's Law (XRD) and ICP-MS (left); and a Comparison of the PtCo NC Size Determined from TEM Images and Calculated Using the Scherrer Equation (XRD) as the Co Content Varies (right)

	% Cobalt (with respect to Pt)			NC size (nm)	
x (x = [Co]/[Pt])	theoretical	XRD	ICP-MS	TEM	XRD
0	0%	0%	0%	2.7 ± 0.4	3.9
0.005	0.5%	1.1%	3.2%	9.8 ± 0.9	8.1
0.009	0.9%	3.4%	5.9%	7.3 ± 1.1	6.5
0.018	1.7%	6.4%	4.7%	5.9 ± 0.7	5.4
0.038	3.7%	8.4%	9.4%	4.7 ± 0.8	4.1
0.095	8.7%	13.9%	17.3%	3.9 ± 0.6	3.3
0.189	15.9%	18.9%	18.5%	2.9 ± 0.5	2.5
0.466	31.8%	25.7%	37.4%	2.3 ± 0.4	2.9

The sizes of the PtCo NCs were determined from XRD using the Scherrer equation, and the values agree well with those obtained from TEM (Table 1). In addition, the peak broadness (fwhm) from the XRD pattern follows the same trend observed in the size distribution obtained by TEM. The NC sizes calculated from the Scherrer equation are smaller than those determined from TEM images. This occurs because XRD provides the average size of the diffracting crystals rather than the particle size, and the intensities of the diffracted XRD peaks scale proportionally with the NC sizes. However, when the NC sizes are smaller than ~2.7 nm (TEM), a slightly larger size is calculated from XRD, which may be attributed to the lack of monodispersity in size, in addition to the low

(37) Reiss, H. *J. Chem. Phys.* **1951**, *19*, 482.
(38) Peng, X.; Wickham, J.; Alivisatos, A. P. *J. Am. Chem. Soc.* **1998**, *120*, 5343.
(39) (a) Nam, K. M.; Shim, J. H.; Ki, H.; Choi, S.; Lee, G.; Jang, J. K.; Jo, Y.; Jung, M.-H.; Song, H.; Park, J. T. *Angew. Chem.* **2008**, *120*, 9646. (b) Cobalt JCPDS no. 15-0806.

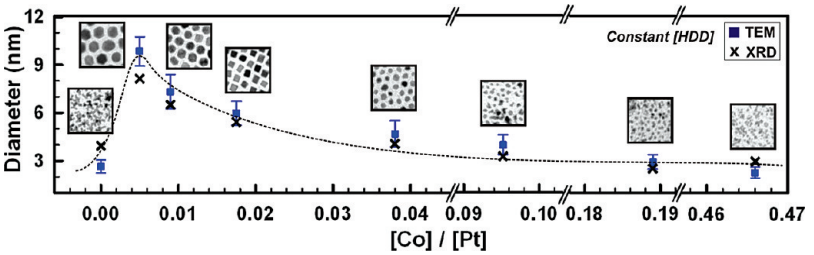

Figure 3. Plot of [Co]/[Pt] versus NC diameter (nm) obtained from TEM (solid blue squares) and XRD (X). Note that there is a dotted line drawn and a scale break in the *x*-axis to better represent the decreasing trend in the PtCo NC sizes.

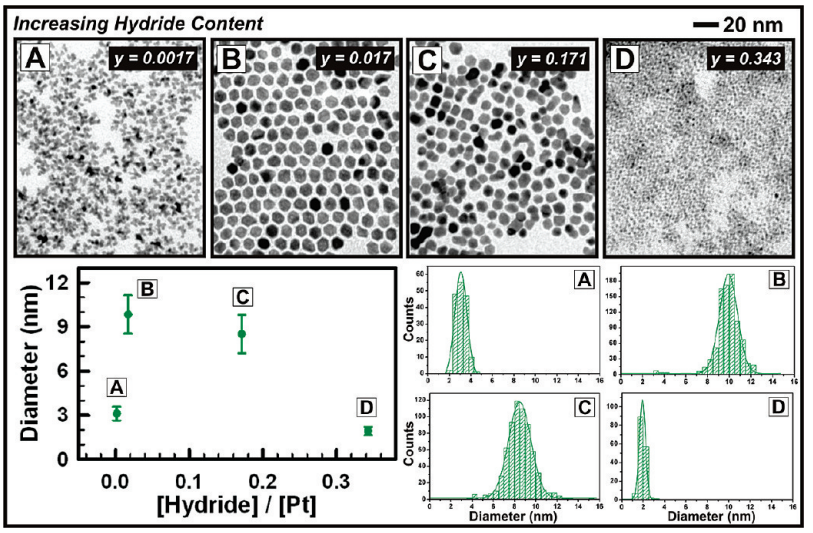

Figure 4. Pt NCs synthesized with increasing hydride concentrations while maintaining constant HDD and Pt precursor concentrations. The [Hydride]/[Pt] ratio is represented by *y*. Top panel: TEM images; Bottom Panel: A plot of [Hydride]/[Pt] versus Pt NCs size (nm) (left) and statistical size analyses (right).

signal-to-noise ratio and peak broadening of the XRD pattern, biasing toward larger size estimation.

The obtained morphologies with increasing [Co]/[Pt] ratio can be divided into three regimes (Figure 3). First, in the absence of Co, polypods were consistently observed. In this regime, the slow reduction rate of HDD leads to a large amount of monomer that simultaneously crystallizes into a large number of reduced Pt nuclei, which are in close proximity to each other, resulting in the subsequent *cementation* of the growing nuclei into polypod structures (Scheme 1).[29] Second, the addition of Co into the synthesis changed the morphology from polypods to spherical/cubic PtCo NCs because of the reduction competition between HDD and Co. In this case, the presence of Co leads to a fast reduction of a portion of the Pt monomers and the formation of a smaller number of nuclei, which are too widely distributed to coalesce, thus enabling growth toward larger sizes. Note that the Pt conversion rate is similar to that in the polypod case. One could argue that the presence of the stronger reducer increases the amount of reduced Pt, leading to large particles, but this is not the case as illustrated by ICP-MS. With the progressive increase in Co content, a fast homogeneous reduction of more Pt monomers occurs, in a sense faster but equivalent to the HDD reduction, causing the appearance of irregular and flake-like NCs which are comparable to the polypod NCs morphology (Scheme 1). It is imperative to point out that having a high concentration of Co does not lead to shape control, which illustrates their concentration limit and the importance of having an appropriate combination/amount of reducers in a synthesis. In other words, the NC size and shape is determined by the relative concentrations, ratios, and reducing strengths (which also depend on temperature) of the reducers. Thus, the same trends should still be observed under different conditions, but offset to smaller or larger NC sizes.

Increasing Hydride Content. As a control experiment, we examined the role of the second reducer by replacing Co with a stronger reducer, lithium triethylborohydride ($H_2/2H^-$, $E°_{red} = -2.25$ V[35]). Figure 4 shows a representative set of TEM images, a plot of NC size versus [Hydride]/[Pt] ratio, and their corresponding statistical size distribution analysis. The increase in hydride concentration is represented by the value of y = [Hydride]/[Pt]. Also, unlike the PtCo alloys produced when using Co as the second reducer, the NCs produced in this case are purely Pt NCs.

The results show morphological trends which are similar to those previously observed when using Co, confirming the competitive reducing role between HDD and the hydride. When $y = 0.0017$ (Figure 4A), the HDD reducer still dominates, resulting in the polypod structures similar to those seen in Figure 1A, with an average NC size of 3.1 ± 0.5 nm. When y was 10 times higher ($y = 0.017$), cuboctahedral Pt NCs of 9.8 ± 1.3 nm were observed (Figure 4B). Since in this case

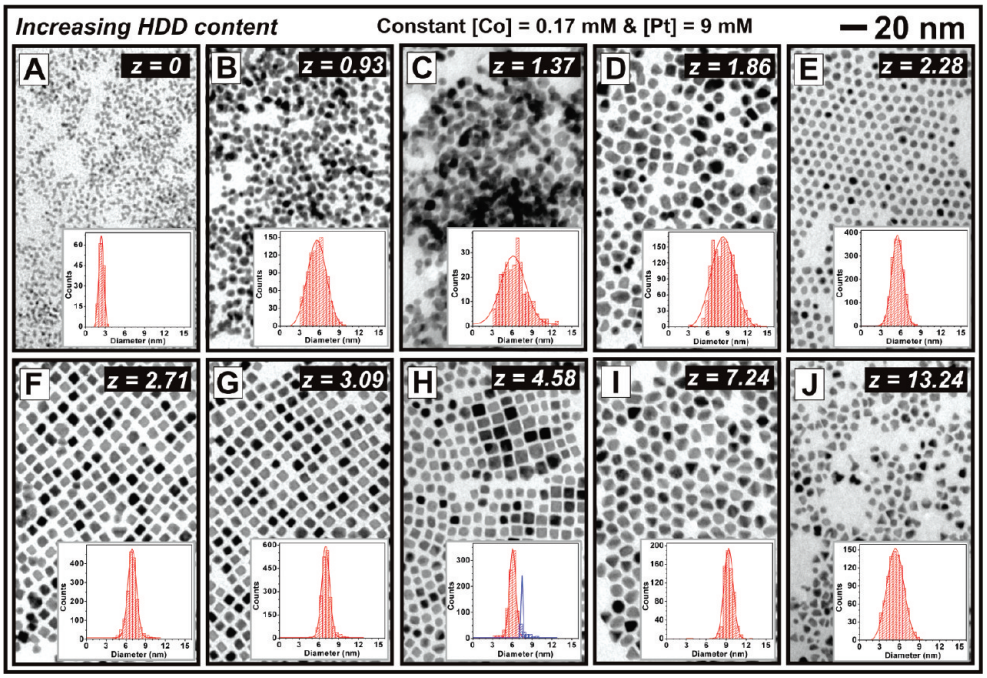

Figure 5. TEM images and the corresponding statistical size analysis of the PtCo NCs synthesized with increasing HDD concentrations while maintaining constant Co and Pt precursor concentrations. The [HDD]/[Pt] ratio is represented by z.

there was no shape-directing agent to promote cube formation, Pt cuboctahedrons which minimized surface and crystal energy were observed.[29] When y was further increased to 0.171 (Figure 4C), fewer cuboctahedron-shaped Pt NCs along with polydispersed spherical NCs were observed (8.5 ± 1.3 nm). This morphology is different from the flake-like PtCo NCs seen in Figure 1G, which were synthesized using a similar [reducer]/[Pt] ratio (x = 0.189). The differences can be attributed to the different reducing strengths of Co and hydride. When hydride was used as the sole reducer (Figure 4D), there was no reducing competition, and as a result, densely packed cemented Pt NCs were obtained (1.9 ± 0.3 nm). The [Hydride]/[Pt] ratio versus diameter plot summarizes a change in the Pt NC size as the hydride concentration increases, showing a trend similar to Figure 3. The subtle differences in the polypod morphology in Figures 4A and 4D signify that the different reducing strengths of HDD and hydride produce dissimilar polypod structures.

Increasing HDD Content. To examine the role of HDD, we vary the amount added to the synthesis while maintaining constant Co and Pt precursor concentrations. Figure 5 shows a representative set of TEM images and the corresponding statistical size analyses as z (z = [HDD]/[Pt]) varies from 0 to 13.24. A flake-like morphology was observed at z = 0 (Figure 5A), again illustrating the characteristic shape produced when only one reducer, in this case, Co, is present in the synthesis. In a control experiment, solely oleylamine (without HDD or Co) under these same synthesis conditions did not have any detectable reducing power, indicating that it was used mainly as a surfactant to avoid NC aggregation during growth. By introducing different amounts of HDD, the emergence of PtCo NCs in the form of aggregated spheres (Figures 5B−C) to a mixture of shaped NCs (Figures 5D-E), and eventually monodispersed cubic NCs were observed (Figures 5F−H). The appearance of two NC size species at z = 4.58 is interesting, as this is different from our typical syntheses, where only one NC size is normally observed. The continued increase in HDD concentration led to the appearance of oval and triangular shaped NCs (Figures 5I and J) instead of the previously seen flake-like NCs, showing the high degeneracy of the system.[29] Thus, our results show that it is not just the differential reducing rate, but also the absolute rate which tunes and affects the NC morphology. The fwhm obtained from the fitted Gaussian functions from the statistical size analysis indicate an initial increase in size dispersion with a subsequent decrease because of the formation of monodispersed cubic NCs, followed by another increase when the HDD concentration was high (Supporting Information, Figure S4).

These NCs were also analyzed using XRD, confirming the crystalline structure of the PtCo NCs as the [HDD]/[Pt] ratio increased (Figure 6). Since the Co concentration was constant in all syntheses, the % of Co (with respect to Pt) calculated using Vegard's law oscillates between 2 and 5%, values which are close to the theoretical % Co added to the synthesis and of that determined from ICP-MS (Supporting Information, Table S1). In addition, there is no particular trend apparent between the % Co and z value, showing that in a high HDD concentration environment, the Co plays a less significant role, where even if all of the metallic Co is oxidized during the reduction of the Pt ions, it probably does not happen at the desired moment.[29] Besides, the high concentration of HDD in the solution may passivate the Co surface, thus preventing the Co NCs from oxidizing, making them less active, showing the high degree of versatility of these syntheses. Similarly, NC sizes were

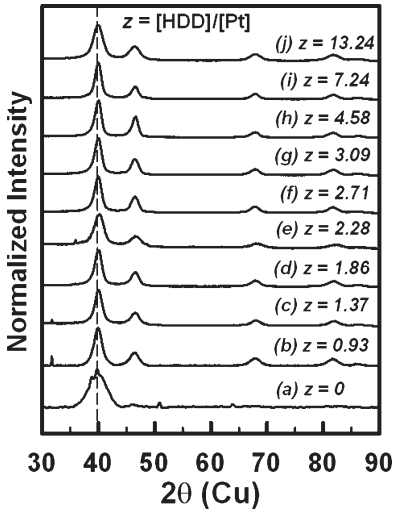

Figure 6. XRD patterns for the PtCo NCs synthesized in the presence of increasing HDD content (z = [HDD]/[Pt]) with constant HDD and Pt precursor concentrations.

Table 2. Comparison of the PtCo NC Sizes Obtained from TEM Images and Calculated Using the Scherrer Equation (XRD) as the HDD Content Varies

	NC size (nm)	
z (z = [HDD]/[Pt])	TEM	XRD
0	2.4 ± 0.3	2.9
0.93	5.7 ± 1.3	5.1
1.37	6.5 ± 1.9	5.8
1.86	8.4 ± 1.7	6.5
2.28	5.5 ± 0.9	4.7
2.71	6.9 ± 0.9	6.5
3.09	7.1 ± 0.8	6.5
4.58	5.9 ± 0.6	6.5
	8.0 ± 0.9	
7.24	9.4 ± 0.8	6.5
13.24	5.4 ± 1.2	4.7

determined from the Scherrer equation and compared with the sizes obtained from TEM images. As shown in Table 2 and Figure 7, the sizes calculated are remarkably close, again illustrating good agreement between the two techniques. The Scherrer equation gave a NC size of 6.5 nm for the bimodal cubes observed at z = 4.58, confirming that XRD provides an average size of all NC. HRTEM of the two size domains shows the presence of perfect cubes along with orthorhombic NCs, both with {002} lateral facets (Supporting Information, Figure S5).

An assessment of the different PtCo NC morphologies synthesized using various HDD concentrations is summarized in Figure 7, where two regimes are observed. When there was no HDD present and Co was the sole reducer, flake-like NCs, which are slightly different from the polypods, were observed. When there was a mixture of HDD and Co, the effects of competitive reducing were observed as prismatic, aggregated spheres, and cubic NCs appeared. The emergence of cubic NCs at a certain [HDD]/[Pt] ratio (z = 2−5) illustrates the importance of having an appropriate combination of Co trace and HDD in the synthesis. When z > 5, the cubic NCs were replaced by oval and triangular shaped NCs because of the dominating influence of the HDD. It is likely that the

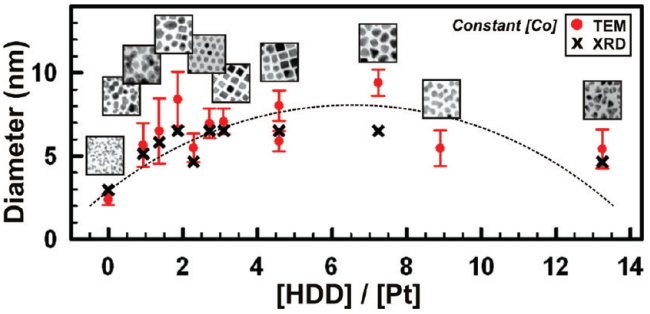

Figure 7. Plot of [HDD]/[Pt] versus PtCo NC diameter (nm) obtained from TEM (solid red circle) and XRD (×). A dotted line is drawn to illustrate the change in NC size.

role of HDD might be limited to not only a reducer but also a surfactant that binds to both the Pt NC and the Co NC surfaces.

To confirm that the oval and triangular shapes observed were due to the dominating role of HDD, two syntheses containing only HDD as the reducer (without Co) were prepared. When the HDD concentration was low (Figure 8A), polypods were observed because of the slow reduction of Pt ions. When the HDD concentration was increased (Figure 8B), the overwhelming concentration of HDD resulted in a mixture of oval, triangular, and rod shaped Pt NCs, confirming the dominating reducing role of HDD.

In addition, the mixture of shaped NCs observed at z = 1.86 was further examined using HRTEM to observe the crystalline structure of the various NCs. In general, the NCs show a degree of coalescence with the neighboring NCs, along with others displaying dislocations or grain boundaries (Figure 9A).

Figure 9B illustrates the first example of the selected NCs which corresponds to a 7.4 nm cuboctahedron. The cuboctahedron is faceted regularly by its {111} and {002} planes. The inner square of dark contrast that we find rotated by 45° in the middle of the experimental cube (marked with dashed lines) demonstrates the cuboctahedral morphology, which is typical in face-centered cubic (fcc) noble metals such as Au, Pt, and Pd. The cuboctahedron in the experimental HRTEM image is visualized along the [001] zone axis. Notice that the 3D supercell model created (with 24739 Pt atoms) has been rotated about different zone axes to allow a better understanding of its morphology, and the rotation that corresponds to the experimental cube is represented by the square drawn in red. The HRTEM examples in Figure 9C and 9D show irregular shaped cuboctahedrons with faceting also occurring on the {111} and {002} planes, however not regularly. Both experimental NCs are visualized along the [110] zone axis, and the corresponding simulations are highlighted in red, containing 6317 and 9201 Pt atoms, respectively. The last example corresponds to a 6.6 nm PtCo sphere, with 10005 Pt atoms in the simulated model (Figure 9E). The NC found experimentally is observed along the [111] zone axis with the model highlighted in red. High ordered facets, especially NCs containing the {111} facet are appealing for applications in fuel cell catalysis.[30]

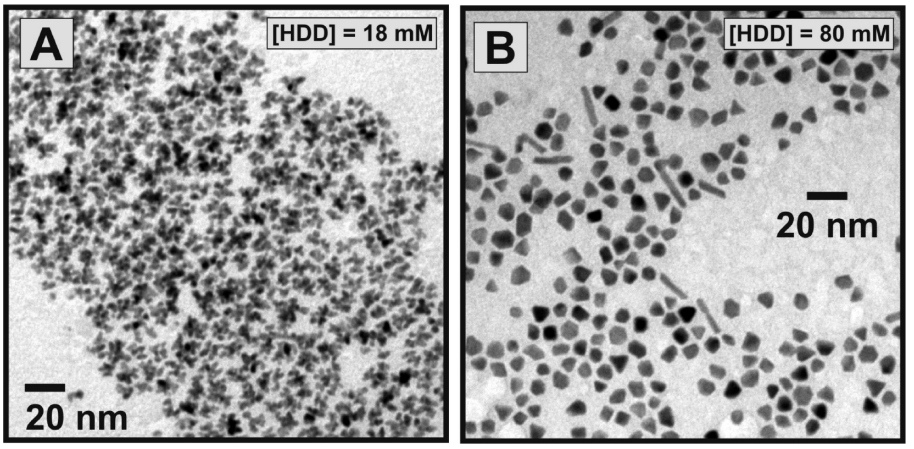

Figure 8. TEM images of Pt NCs synthesized in the presence of HDD at low (A) and high (B) concentration.

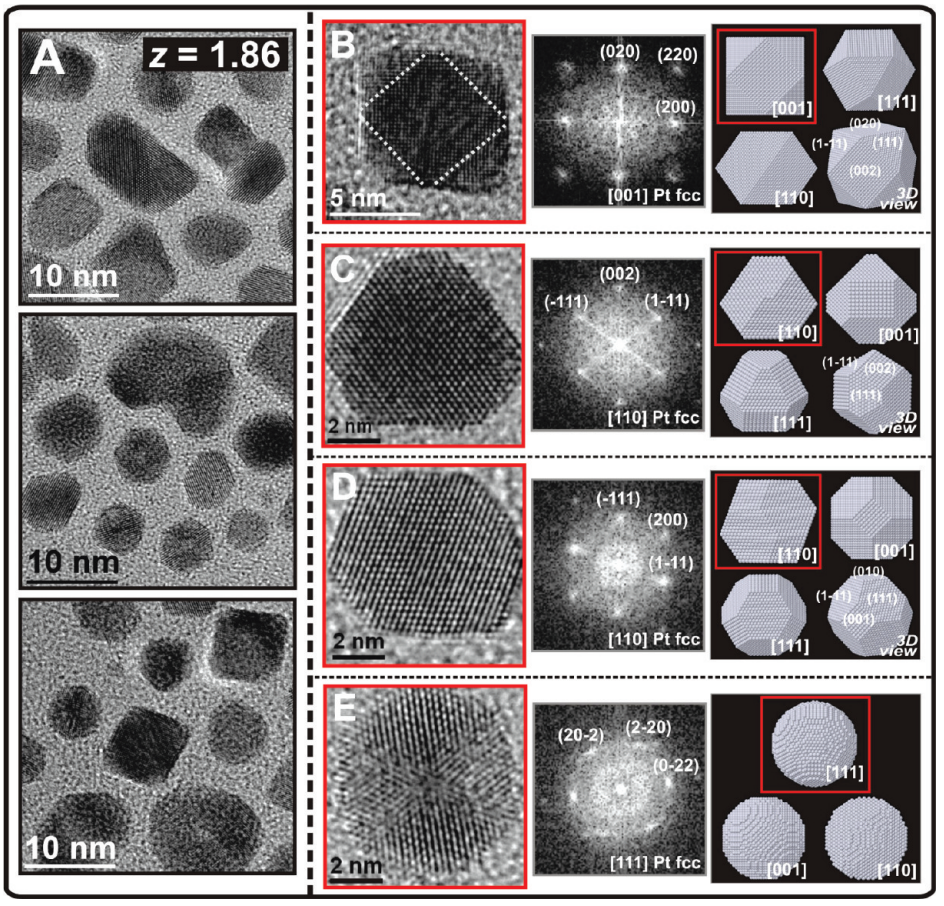

Figure 9. Panel of HRTEM images for the NCs synthesized at $z = 1.86$: mixture (A) and selected NCs (B-E) with their corresponding FFT patterns and simulated 3D supercell atomic models. The red square drawn on the simulated model represents the visualized zone axis of the HRTEM experimental image.

Conclusions

The synthesis of Pt (and PtCo alloy) NCs in the presence of one or two reducing agents was examined in this work. Upon the addition of Pt precursor, an initial burst of nucleation of small, amorphous Pt nuclei results in a dramatic decrease in the concentration and availability of the Pt precursor, and thus opens a gateway for the NC growth phase. The existence of both freshly formed nuclei and precursor at the beginning of the synthesis reaction represents a highly susceptible and vulnerable stage, where the size and shape of the NCs can be easily manipulated.[40] In which case, a simple manner by which one can alter the relative concentrations of available precursor and the growing nuclei to have an impact on the growth kinetics is by mixing reducers at relative concentrations such that they compete to reduce

(40) Zheng, H.; Smith, R. K.; Jun, Y.; Kisielowski, C.; Dahmen, U.; Alivisatos, A. P. *Science* **2009**, *324*, 1309.

the Pt ions. Our results showed that when only one reducer was present in the synthesis, polypod-type morphology was observed. The dissimilar features of the polypods (flakes or cemented NCs) can be attributed to which dominating reducer was added to the synthesis. When the synthesis contained two competing reducers, shaped NCs were obtained. This study illustrates another synthetic approach where different morphologies (size and shape) can be produced by taking advantage of the susceptibility of the system to minor changes during the early reaction stages. Part of our ongoing work includes characterization of the Co distribution on the Pt surface, by probing the chemical states and depth profile of the alloy NCs to elucidate the role of metallic Co in the shape control.

Acknowledgment. This work is supported by the Spanish MICINN. S.L. acknowledges the support of the Beatriu de Pinós fellowship from the Catalan Government. M.V. acknowledges the support from project: MAT2006-13572-C02-02. The authors thank Serveis Cientificotecnics of Universitat de Barcelona for the use of their TEM equipment.

Supporting Information Available: Additional HRTEM and TEM images, plots of fwhm versus increase in the reducer/Pt ratio and comparison on the % Co using EDX, XRD, and ICPMS. This material is available free of charge via the Internet at http://pubs.acs.org.